Photon avalanche upconversion in Tm^{3+}-doped fluoroindogallate glasses

2002 J. Phys.: Condens. Matter 14 5651

(http://iopscience.iop.org/0953-8984/14/23/301)

INSTITUTE OF PHYSICS PUBLISHING JOURNAL OF PHYSICS: CONDENSED MATTER

J. Phys.: Condens. Matter **14** (2002) 5651–5663 PII: S0953-8984(02)30317-5

Photon avalanche upconversion in Tm^{3+}-doped fluoroindogallate glasses

M J V Bell[1], D F de Sousa[2], S L de Oliveira[2], R Lebullenger[2], A C Hernandes[2] and L A O Nunes[2]

[1] Departamento de Física, Universidade Federal de Juiz de Fora, Juiz de Fora-MG 36036-330, Brazil
[2] Instituto de Física de São Carlos, USP, Caixa Postal 369, São Carlos-SP, Brazil

Received 29 October 2001, in final form 31 January 2002
Published 30 May 2002
Online at stacks.iop.org/JPhysCM/14/5651

Abstract

In this work, a study of photon avalanche at 476 nm ($^1G_4 \rightarrow {}^3H_6$) in Tm-doped fluoroindogallate glasses is reported. Transient Tm^{3+} emissions at 476, 450 nm ($^1D_2 \rightarrow {}^3F_4$) and transmission at the pumping wavelength (645 nm) were monitored as a function of excitation power and Tm^{3+} concentration. We propose a theoretical treatment based on a set of five non-linear coupled rate equations, which include sequential two-photon absorption (TPA), two cross-relaxations among Tm^{3+} ions, and energy migration at the $^3F_4$ metastable state. It is demonstrated that energy migration in highly doped samples plays a fundamental role in the photon avalanche process, and may even suppress it. Additionally, sequential TPA must be considered in order to explain the transient behaviour of the 450 nm emission in the photon avalanche regime.

1. Introduction

Upconversion of infrared into visible photons has been a successful approach to achieving lasers in the blue-green region for use in optical data storage, colour displays, bar-code reading, etc [1]. Among the several upconversion mechanisms, the most studied are sequential two-photon absorption (TPA), 'addition de photons par transfert d'energie' (APTE), and photon avalanche (PA). The contribution of each one in the generation of the upconverted light depends on pumping wavelength, light intensity, temperature, and phonon energies of the matrix.

TPA consists of ground-state absorption (GSA) followed by excited-state absorption (ESA) from an intermediate state to the upper upconversion level. APTE involves energy transfer between two ions in the intermediate state resulting in the promotion of one ion to the upper level and the other to the ground state. The PA regime may be achieved if the following processes occur: off-resonance GSA at the pumping light followed by ESA at the same energy; the presence of metastable intermediate states and efficient cross-relaxation (CR) mechanisms to populate these intermediate states. Two experimental consequences of PA are a

critical slowing down of the metastable level rise time and a sudden increase in the upconverted emission above a laser power threshold [2].

Chivian *et al* [3] first observed the PA effect in 1979 when investigating an infrared quantum counter-process in $LaCl_3$ and $LaBr_3$ crystals doped with Pr^{3+}. The phenomenon has attracted considerable attention due to its potential applications in generating upconverted light [4–8]. PA laser action has been observed in a wide range of rare-earth-doped materials [2, 9, 10]. In particular, Tm^{3+} ions are interesting as they can be excited by red photons in the range from 620 to 650 nm, provided by diode lasers, and give rise to blue emission at 476 nm [2, 11]. PA mechanisms in Tm^{3+} ions have been treated microscopically using mean-field theories and rate equations [12] involving four levels and two cross-relaxations among Tm ions, or the density matrix approach describing the non-linear susceptibility of the system [13]. Contributions of temperature and wavelength pumping have also been reported [14]. Nevertheless, the effects of Tm concentration and TPA on PA have not been considered in detail.

The present paper investigates PA upconversion in Tm^{3+}-doped fluoroindogallate glasses. These glasses are interesting as upconversion media because they incorporate large dopant concentrations, and present 90% transmittance in the 200–8000 nm wavelength range for a sample 3 mm thick and phonon energies of about 500 cm^{-1} [15]. Transient blue emissions at 476 nm ($^1G_4 \rightarrow {}^3H_6$) and 450 nm ($^1D_2 \rightarrow {}^3F_4$) were measured as a function of incident laser power and Tm^{3+} concentration, with excitation at 645 nm. Transient transmission measurements at the pumping wavelength were also performed. We show that the avalanche regime is achieved and it may be understood in terms of five-level rate equations, which differ from the previously reported ones because they include two TPA processes and energy migration of the $^3F_4$ metastable level. We show that Tm concentration is a critical parameter for PA to occur. For high doping levels, upconversion at 476 nm is quenched, the $^3F_4$ metastable state lifetime decreases, and PA is not observed.

2. Experimental set-up

The samples have the following molar compositions: $15InF_3$–$20GaF_3$–$30PbF_2$–$15ZnF_2$–$(20 - x)CaF_2$–$xTmF_3$ with $x = 1$, 2, 4, and 7 (hereafter called xTm). The details concerning the preparation of fluoroindogallate glasses were given in [15]. For Tm-doped samples, Tm_2O_3 (3N) was transformed into anhydrous fluoride using NH_5F_2 under a dry atmosphere. The room temperature rise-time measurements were performed with a dye laser (DCM) operating at 645 and 660 nm, pumped by an Ar^+ laser. Modulated operation was achieved using a chopper, locked at 8 Hz. The transient blue emissions at 476 and 450 nm, corresponding to the $^1G_4 \rightarrow {}^3H_6$ and $^1D_2 \rightarrow {}^3F_4$ Tm^{3+} transitions, were analysed by a 0.25 m simple monochromator coupled to a standard photomultiplier, and were acquired by a digital oscilloscope. Transient transmissions at 645 and 660 nm were simultaneously recorded by another photomultiplier connected to the same digital oscilloscope. Steady-state blue emissions as a function of laser power were collected by a photomultiplier coupled to a lock-in amplifier. The laser excitation power was in the range from 40 to 400 mW. All measurements were performed at room temperature.

3. Results

Figure 1 shows the energy levels obtained from the absorption spectrum of the 1Tm sample and were ascribed following the notation of [10]. Some pumping mechanisms, with rates R_1,

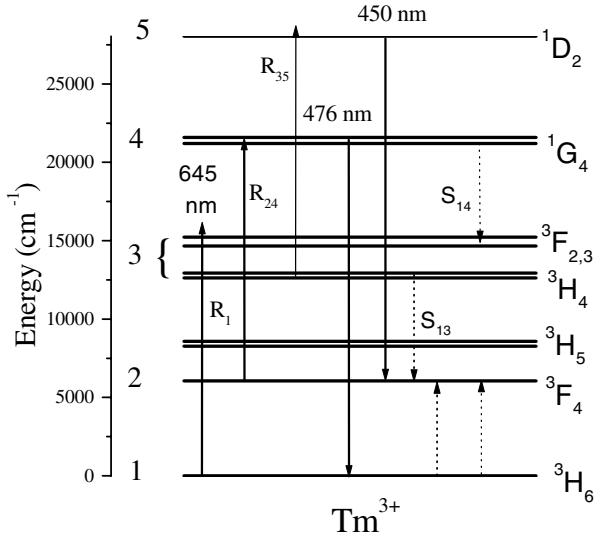

Figure 1. Energy levels of Tm^{3+} ions, showing some pumping routes (at 645 nm) and relevant radiative emissions at 450 and 476 nm. S_{13} and S_{14} stand for rates of cross-relaxations, while R_1, R_{24}, and R_{35} indicate pumping rates.

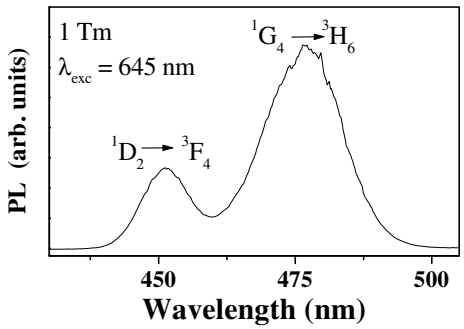

Figure 2. Radiative emission in the range from 430 to 510 nm from the 1Tm sample pumped at 645 nm, indicating the $^1G_4 \rightarrow {}^3H_6$ and $^1D_2 \rightarrow {}^3F_4$ Tm^{3+} transitions centred at 476 and 450 nm, respectively.

R_{24}, and R_{35} (continuous curves), and cross-relaxations among Tm ions, with rates S_{13} and S_{14} (dotted curves), are also shown. According to the figure, pumping at 645 nm is resonant with the $^3F_4 \rightarrow {}^1G_4$ Tm^{3+} ESA (R_{24}) and nearly resonant with the $^3H_4 \rightarrow {}^1D_2$ Tm^{3+} ESA (R_{35}).

Figure 2 displays steady-state photoluminescence (PL) emission in the blue range from 430 to 510 nm for sample 1Tm pumped at 645 nm. The two bands centred at 450 and 476 nm were attributed to the $^1D_2 \rightarrow {}^3F_4$ and $^1G_4 \rightarrow {}^3H_6$ Tm^{3+} transitions, respectively. Additionally, it was observed that both bands decrease in size as the Tm concentration increases, indicating the presence of efficient quenching mechanisms.

Figure 3 shows the normalized transient PL intensity of the $^1G_4 \rightarrow {}^3H_6$ ((*a*)–(*c*)) transitions, the $^1D_2 \rightarrow {}^3F_4$ ((*d*)–(*f*)) transitions, and the normalized transient transmission of the incident laser ((*g*)–(*i*)) for the *x*Tm samples, as a function of laser power. Spectra were obtained by exciting the samples by a square wave (8 Hz) at 645 nm and excitation powers of

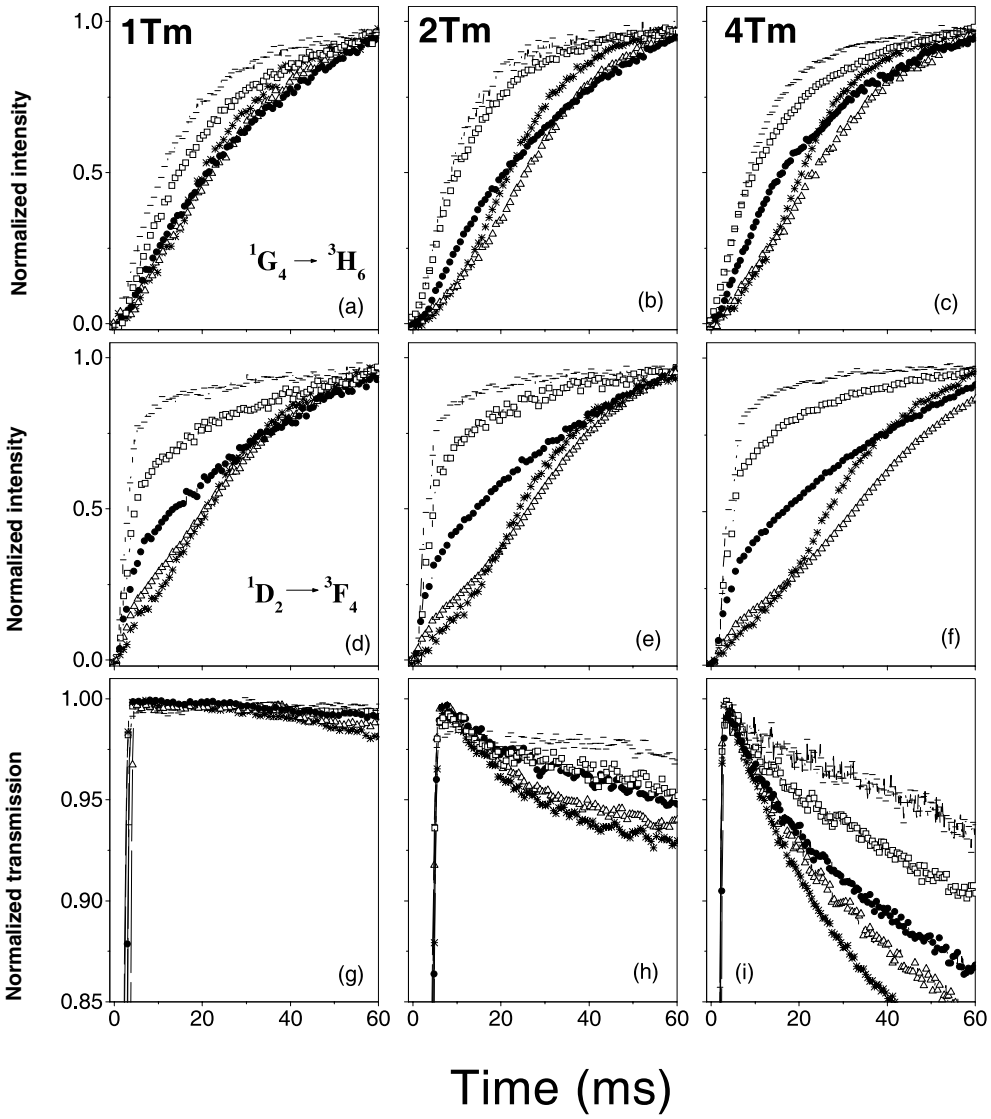

Figure 3. ((*a*)–(*c*)) The rise time of the $^1G_4 \rightarrow {}^3H_6$ transitions, ((*d*)–(*f*)) that of the $^1D_2 \rightarrow {}^3F_4$ Tm^{3+} transitions, and ((*g*)–(*i*)) the transient transmission, pumped at 645 nm, as a function of the incident laser power for samples *x*Tm. The laser powers are 40 mW (−), 100 mW (□), 200 mW (●), 300 mW (△), and 400 mW (*).

40, 100, 200, 300, and 400 mW focused by a 3 mm microscope lens. According to the figure, the curve shapes of the 476 and 450 nm emissions as well as the transmission depend on the laser power for concentrations up to 4 mol% of Tm. In particular, transmission for $t \rightarrow \infty$ decreases as the laser power increases. This is indicative of negative non-linear absorption [16]. The results for sample 7Tm are not shown. They do not exhibit any laser power dependence and rise times are about 5 ms for emissions at 450 and 476 nm.

Figure 4(*a*) depicts the rise time of the 476 nm emission obtained from figure 3 for samples 2Tm and 4Tm, which exhibited the most pronounced curve shape dependences on the power

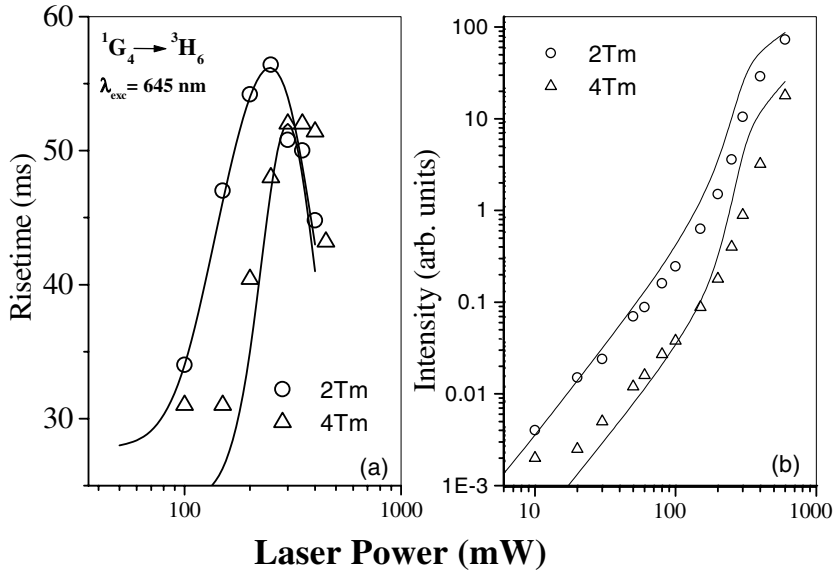

Figure 4. (*a*) The rise time of the 476 nm emission obtained from figure 3 and (*b*) the integrated PL intensity of the 476 nm emission, as a function of laser power, for the 2Tm and 4Tm samples.

excitation. The rise time was defined as the time taken to reach 90% of the steady-state intensity of the $^1G_4 \rightarrow {}^3H_6$ transition. It can be seen that the rise time increases for excitation powers up to 200 mW (sample 2Tm) and 300 mW (sample 4Tm); this is followed by a slowing down for higher laser powers. According to figure 4(*a*), the maximum rise time is about 55 ms (sample 2Tm), while the lifetime of the $^3F_4$ level is 11.7 ms (for the 1Tm sample). Figure 4(*b*) shows the integrated PL intensity of the 476 nm emission as a function of laser power for the 2Tm and 4Tm samples. A clear non-linear dependence of the intensity on the laser power is seen, as expected in a PA regime. The continuous curves in figures 4(*a*) and (*b*) were obtained from fitting procedures and will be explained in the following section.

4. Discussion

To describe the blue upconversion route in Tm^{3+} ions we propose a set of five coupled non-linear rate equations. This is a macroscopic approach, which considers overall densities without regard to the environment of the ionic species. Such model is valid at high rare-earth concentrations and for samples without cluster formation. The validity of rate equation approach relies on two basic assumptions: fast diffusion and short lifetime (i.e. negligible effect) of levels not included in the scheme [17, 18]. Fast diffusion implies thermalization within the system that is much more rapid than the energy transfer, so in this case a given system distributes energy internally in a time short compared with that taken by transfer to another system. Under this assumption, the usual kinetic non-linear rate equation is derived [19].

In particular, in the PA phenomena, Normand *et al* [20] have demonstrated that the rate equation approach for second-order phase transition, and more generally for bifurcation, is valid except extremely close to the bifurcation point, for which the fluctuations take on great importance. Due to the analogy of PA and second-order phase transition, and as soon as the critical point is not too close, such a mean-field approach is valid to describe PA [21].

Spectral broadening is also considered in the rate equations. The process occurs by site-to-site energy transfer across inhomogeneously broadened line profiles by the two-phonon-assisted process discussed by Holstein *et al* [22]. The resonant optical excitation excites only a group of equivalent sites contributing to a homogeneous line and, due to the site-to-site energy migration, the inhomogeneous line profile is obtained. At room temperature the process referred to is fast compared with any other energy transfer (cross-relaxation or migration of the $^3F_4$ level).

The proposed rate equations take into account the levels numbered from 1 to 5 in figure 1, two cross-relaxations (with rates S_{13} and S_{14}), GSA absorption (with rate R_1), and two different mechanisms for ESA: the R_{24}-mechanism, which is resonant with the $^3F_4 \rightarrow {}^1G_4$ transition (and gives rise to the avalanche effect) and the R_{35}-mechanism, which is nearly resonant with the $^3H_4 \rightarrow {}^1D_2$ transition. The non-resonant GSA populates the $^3F_2$ level; this is followed by a fast non-radiative decay to the $^3H_4$ level (represented by $R_1 n_1$ in the rate equations). From this level, besides the relaxation to the ground state, two paths are possible: one is TPA, which directly populates the $^1D_2$ level, and results in radiative emission at 450 nm. The other gives rise to PA. In this case, the interaction of two neighbouring ions may give rise to the CR (S_{13}): $^3H_4$, $^3H_6 \rightarrow {}^3F_4$, $^3F_4$ populating the $^3F_4$ level. Two ions excited at the $^3F_4$ level may be promoted to the $^1G_4$ level by means of the R_{24}-ESA ($^3F_4 \rightarrow {}^1G_4$). If one excited ion at the $^1G_4$ level interacts with a neighbouring one at the fundamental state, by means of CR (S_{14}): $^1G_4$, $^3H_6 \rightarrow {}^3F_4$, $^3F_2$, then the $^3H_4$ level is populated once again. So, one Tm^{3+} ion in the $^3H_4$ level can produce three ions in the $^1G_4$ level after the resonant R_{24}-ESA, and so on, characterizing the PA effect. The rate equations used to describe this system are given by

$$\frac{dn_1}{dt} = -R_1 n_1 + W_2 n_2 + W_{31} n_3 + W_{41} n_4 - S_{13} n_1 n_3 - S_{14} n_1 n_4 + W_{51} n_5$$

$$\frac{dn_2}{dt} = -R_{24} n_2 - W_2 n_2 + W_{32} n_3 + 2S_{13} n_1 n_3 + S_{14} n_1 n_4 + W_{52} n_5 + W_{42} n_4$$

$$\frac{dn_3}{dt} = R_1 n_1 - R_{35} n_3 - W_3 n_3 + W_{43} n_4 - S_{13} n_1 n_3 + S_{14} n_1 n_4 + W_{53} n_5$$

$$\frac{dn_4}{dt} = R_{24} n_2 - W_4 n_4 - S_{14} n_1 n_4 + W_{54} n_5$$

$$\frac{dn_5}{dt} = R_{35} n_3 - W_5 n_5$$

where n_1, n_2, n_3, n_4, and n_5 are the normalized populations of levels 1, 2, 3, 4, and 5 attributed to the $^3H_6$, $^3F_4$, $^3H_4$, $^1G_4$, and $^1D_2$ Tm^{3+} levels, respectively. R_1, R_{24}, and R_{35} are given by $\sigma I / h\upsilon$, where σ corresponds to the ground or ESA cross-section, I is the incident light intensity, and υ is the incident laser frequency. W_{ij} refers to the rate of radiative decay from level i to j, except for level 2, and its values were obtained from standard Judd–Ofelt calculations [23]. W_i is the summation of the radiative decay rates from level i over all j-levels below i.

The efficiency of the cross-relaxations with rates S_{13} and S_{14} is demonstrated in figures 5(a) and (b), which show the intensities of the $^1G_4 \rightarrow {}^3H_6$ and $^3H_4 \rightarrow {}^3H_6$ Tm^{3+} transitions, as a function of Tm^{3+} concentration, when resonantly pumped at 476 and 778 nm, respectively. It can be noted that both intensities decrease for high Tm^{3+} concentration. These results corroborate the use of S_{13} and S_{14} in the rate equations and are in agreement with [27–29].

As regards the $^3F_4$ metastable level (level 2 in the rate equations), its lifetime was measured as a function of Tm^{3+} concentration. The observed decay curves were exponential with lifetimes varying from 11 (1Tm sample) to 2.4 ms (7Tm sample). On the other hand, the radiative lifetime for the $^3F_4$ level obtained from the Judd–Ofelt calculations is

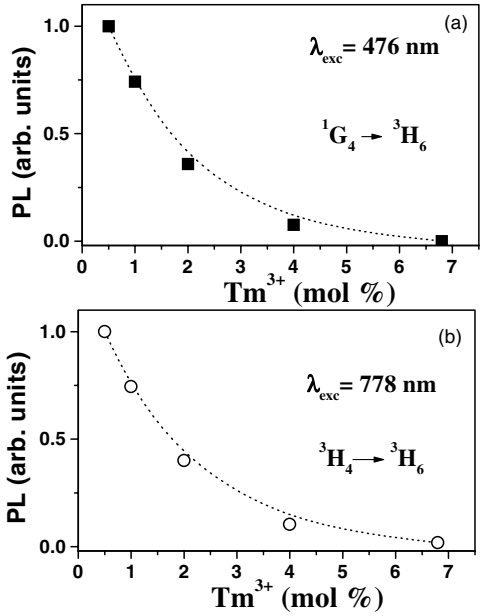

Figure 5. PL emission from the (*a*) $^1G_4 \rightarrow {}^3H_6$ and (*b*) $^3H_4 \rightarrow {}^3H_6$ Tm^{3+} transitions, resonantly pumped at 457 and 778 nm, respectively, as a function of Tm^{3+} concentration.

about 8.8 ms. Such discrepancy is due to other mechanisms which take place as the Tm concentration is increased: for example, energy migration between Tm ions and energy transfer to unintentionally introduced defects in the matrix. This energy migration was taken into account using W_2 as the inverse of the measured $^3F_4$ lifetime.

The rate equations were solved to fit the rise curves of the $^1G_4 \rightarrow {}^3H_6$ ($n_4(t)$), $^1D_2 \rightarrow {}^3F_4$ ($n_5(t)$) transitions and the transient transmission of the incident laser, as can be seen in figures 6(*a*)–(*i*). The agreement between simulated and experimental curves is quite good, as all the features were well reproduced. The following Judd–Ofelt parameters [23] were used: $W_{31} = 700\ s^{-1}$, $W_{32} = 80\ s^{-1}$, $W_{41} = 550\ s^{-1}$, $W_{42} = 120\ s^{-1}$, $W_{43} = 30\ s^{-1}$, $W_{51} = 6000\ s^{-1}$, $W_{52} = 6000\ s^{-1}$, $W_{53} = 200\ s^{-1}$, $W_{54} = 200\ s^{-1}$. W_2 was obtained from the inverse of the experimental $^3F_4$ level lifetime. R_1, R_{35}, and q, defined as $q = R_1/R_{24}$, were considered as adjustable parameters. The cross-relaxation rates S_{13} were obtained from time-resolved measurements of the $^3H_4$ level [24]. Moreover, we considered $S_{13} = S_{14}$ for all samples, on the basis of the similar quenching behaviours of the $^3H_4$ and $^1G_4$Tm levels, shown in figures 5(*a*) and (*b*). Contributions from multiphonon rates to the W_{ij}-parameters were neglected. This assumption was based on the gap law: $W_{NR} = W_{NR}(0)\exp(-\alpha\,\Delta E)$, where $W_{NR}(0)$ and α are positive constants, characteristic of the host, and ΔE is the gap difference. The lowest-energy gap in this system, at about 4400 cm^{-1}, is given by the $^3H_4 \longrightarrow {}^3H_5$ transition. The corresponding multiphonon relaxation rate, W_{NR}, can be estimated using the values for α (5.8×10^{-3} cm^{-1}) and $W_{NR}(0)$ ($1.9 \times 10^{10}\ s^{-1}$), for fluoride glasses. Considering that these glasses have low phonon energy (about 500 cm^{-1}), about nine phonons are necessary to produce multiphonon de-excitation. Consequently, a negligible multiphonon probability for the $^3H_4$ level is estimated [25].

The relation between the laser power, P (in mW), and the pumping rates, R_1 and R_{35}, were given by $R_1 = 2.5 \times 10^{-3}\ P$ and $R_{35} = R_{24}/2$, while $q = R_1/R_{24} = 8 \times 10^{-3}$, and were

Table 1. Parameters S_{13}, S_{14}, lifetimes of the $^3F_4$ level ($\tau_{^3F_4}$), and W_2 ($=1/\tau_{^3F_4}$) used in the rate equations.

Sample	$\tau_{^3F_4}$ (ms)	W_2 (s^{-1})	S_{13} (s^{-1})	S_{14} (s^{-1})
1Tm	11.7	85	1 000	1 000
2Tm	9.5	105	10 000	10 000
4Tm	6.2	161	100 000	100 000
7Tm	2.4	416	350 000	350 000

fixed for all samples. Table 1 shows the results for S_{13} and S_{14}, the $^3F_4$ level lifetime, and the W_2-parameter as a function of Tm concentration, used in the rate equations. The accuracies of the numerical parameters are estimated as 5% (for q), 20% (for W_{ij}, S_{13}, and S_{14}), and 50% (for R_{35}).

The influence of the cross-relaxations used in the simulations is clear. As S_{13} and S_{14} increase (with all other parameters fixed), the lineshapes of rise curves $n_4(t)$ and $n_5(t)$ become strongly non-exponential and exhibit a bending point. If S_{13} is set to zero, there is no rise-time dependence on the laser power for any sample and any emission. In other words, there is no PA effect. Furthermore, if S_{14} is not taken into account, the rise time of the 450 nm emission is always fast, independently of the Tm concentration and laser power. This corroborates the double-cross-relaxation model used in this work and those previously reported [9]. Other cross-relaxation energy transfers: $^1D_2$, $^3H_6 \longrightarrow {}^3H_4$, $^3F_{2,3}$; $^1G_4$, $^3H_6 \longrightarrow {}^3H_4$, $^3H_5$; and $^1D_2$, $^3H_6 \longrightarrow {}^1G_4$, $^3F_4$ were included in our rate equations and they did not significantly change the lineshapes shown in figure 6. Hence, they were neglected.

The $^1D_2$ pumping mechanism (R_{35}) must be considered, as the emission intensities at 450 and 476 nm are comparable in all cases (see figure 2), and its inclusion leads to adequate prediction of the $^1D_2$ emission as a function of Tm concentration and laser power. In this way, the evolution of the lineshapes of the $^1D_2$ emission can be understood as follows. For low laser powers, sequential TPA is the main pumping route for $^1D_2$ population, as can be seen from the low rise time in this case. On the other hand, as the laser power increases, the rise curves of the $^1D_2$ emission are modified. This indicates that a new four-step mechanism is operative: (1) GSA followed by non-radiative relaxation to the $^3F_4$ level; (2) ESA indicated by R_{24} in figure 1, which takes Tm ions to the $^1G_4$ level; (3) cross-relaxation with rate S_{14} resulting in Tm ions at the $^3H_4$ and $^3F_4$ levels; and finally (4) ESA with rate R_{35}, resulting in $^1D_2$ emission.

The best-fitting parameter R_{35} was obtained for the relation $R_{35} = R_{24}/2$. Our estimation is based on two main considerations. One relates to the absorption spectrum of the samples. It can be noted that R_{24}-ESA is resonant at 643, while R_{35}-ESA is resonant at 654 nm. Consequently, the R_{24}-mechanism is almost resonant at the PA pumping, while the R_{35}-mechanism is shifted from resonance. The other consideration is that, according to Kishimoto and Hirao [26], only the $^3H_4 \longrightarrow {}^1D_2$ ESA was detected in a set of glassy hosts. This allows us to suppose that R_{35} is greater than R_{24} in their respective resonance conditions. However, there are very few reports concerning ESA processes in Tm-doped glasses. To our knowledge, Kishimoto and Hirao [26] were the first to publish results on Tm-doped ESA in glasses. So, our estimation is a rough approximation and only means that R_{24} and R_{35} may be of the same order of magnitude at this pumping wavelength (645 nm).

As regards the W_2-parameter, if its dependence on the Tm concentration is not taken into account, the simulation predicts that the avalanche effect is enhanced for highly doped samples. However, the experimental results indicate that PA is not seen for the 7Tm sample.

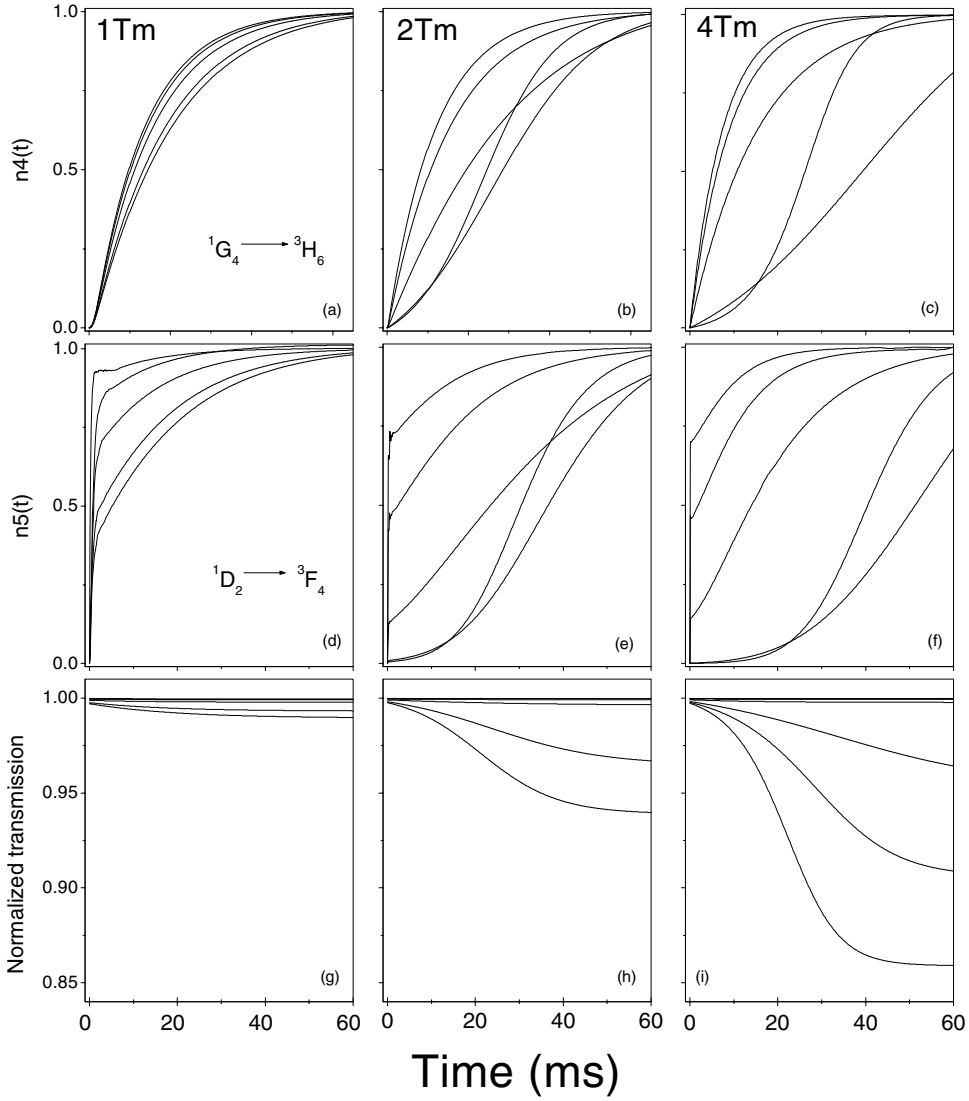

Figure 6. Results of simulation of the experimental curves in figure 3. The pumping rates, R_1, are 0.1, 0.2, 0.5, 0.8, and 1.0 s^{-1}. The parameter q is 0.008. W_2, S_{13}, and S_{14} accord with table 1.

Parameter q is of fundamental importance in evaluating the efficiency of the PA. It has been reported that for $q \ll 1$ [9], PA is observed and manifests itself as a strong increase in the rise time followed by a critical slowing down for intensities above a laser power threshold [9]. Blue emission at 476 nm is also expected to increase abruptly above the threshold. The continuous curves in figures 4(a) and (b) resulted from the rate equations—by taking the rise time and steady-state intensities of the simulated rise curves in figure 6. It can be noted that the theory predicts all the experimental features. Moreover, according with figure 4(a), sample 2Tm presents a threshold at around 150, while sample 4Tm presents one at about 250 mW. This can be understood according to the PA theory [9], which states that the laser power threshold is inversely proportional to the metastable state lifetime. So, as the Tm concentration increases,

Table 2. Comparison of rate equation parameters used in this work and those previously published. The W_{ij} are the Judd–Ofelt parameters giving the rate of radiative decay from level i to level j. σ_{ij} and σ_1 are the ESA cross-sections for levels i to j, and σ_1 is the GSA at the pumping wavelength indicated.

Host	This work	BIGaZYTZr	Fluorozirconate	Tellurite	YAG	Fluoroindate
Reference	—	[30]	[27]	[38]	[8]	[25]
Tm^{3+}	4 mol%	1 mol%			5 mol%	2.5 mol%
λ (nm)	645	—	—	—	628	630
W_{51} (s^{-1})	6000	5806	6586	16 394	—	5667
W_{52} (s^{-1})	6000	6197	8590	41 601	—	6075
W_{53} (s^{-1})	200	783	933	3050	—	781
W_{54} (s^{-1})	200	92	115	1858	—	72
W_{41} (s^{-1})	550	483	628	2238	753	472
W_{42} (s^{-1})	120	95	99	231	752	97
W_{43} s^{-1})	30	102	126	412	245	126
W_{31} (s^{-1})	700	609	683	2116	480	572
W_{32} (s^{-1})	80	70	60	203	105	55
W_2 (s^{-1})	160	123	166	452	—	107
$q = R_1/R_{24}$	8×10^{-3}	—	—	—	5×10^{-4}	3.7×10^{-2}
σ_{35} (cm^2)	3.1×10^{-22}	—	—	—	—	—
σ_1 (cm^2)	5.0×10^{-23}*	—	—	—	1.6×10^{-24}	6.93×10^{-24}
σ_{24} (cm^2)	6.2×10^{-21}	—	—	—	3.2×10^{-21}	1.86×10^{-22}
S_{13} (s^{-1})	100 000	—	—	—	40 000	15 700
S_{14} (s^{-1})	100 000	—	—	—	17 000	39 000

* σ_1 was obtained from the Tm^{3+} absorption spectrum.

resulting in a reduction of the metastable lifetime, the power threshold shifts to higher laser excitations. Figure 4(*b*) shows the upconverted intensity of samples 2Tm and 4Tm, as a function of laser excitation, and reveals a similar threshold behaviour.

In view of the above considerations, the upconverted emission at 476 nm as a function of Tm^{3+} concentration may be understood by considering that, despite the increase of the cross-relaxation rates S_{13} and S_{14}, migration of the $^3F_4$ level diminishes the efficiency of the avalanche process and may even suppress it, as can be concluded from the quenching of the emission at 476 nm for Tm^{3+} concentrations above 1%. Indeed, the PA effect was not observed in the 1Tm sample because of the low-efficiency feeding of the $^3F_4$ level. The same occurs for the 7Tm sample, where energy transfer quenches the $^1G_4$ level emission. The effect is satisfactorily reproduced by the simulations, and a rise time of about 5 ms is observed for both blue emissions (476 and 450 nm). Similar behaviour has been previously reported in Tm^{3+}-doped BIGaZYTZr glasses [30]. Moreover, the residual GSA puts all the Tm^{3+} ions in the metastable $^3F_4$ state whatever the excited-state pumping rate R_{24} is, and also reduces the PA efficiency [31, 32].

Table 2 lists Tm-doped systems with their Judd–Ofelt radiative parameters, as well as the S_{13}-, S_{14}-, and q-parameters reported previously, for comparison purposes. It is important to note that in spite of the great number of reported papers on PA in Tm-doped glasses, some of them are qualitative, so there are not so many PA parameters available [29, 36].

To demonstrate the effect of the GSA, we performed the same measurements with the pumping laser at 660 nm. Results are shown in figure 7. In this case, only the parameter q was changed to $q = 0.9$, while all other parameters remained fixed. It can be seen from the figure that the PA effect does not exist, because at 660 nm the GSA is nearly resonant and $q \sim 1$.

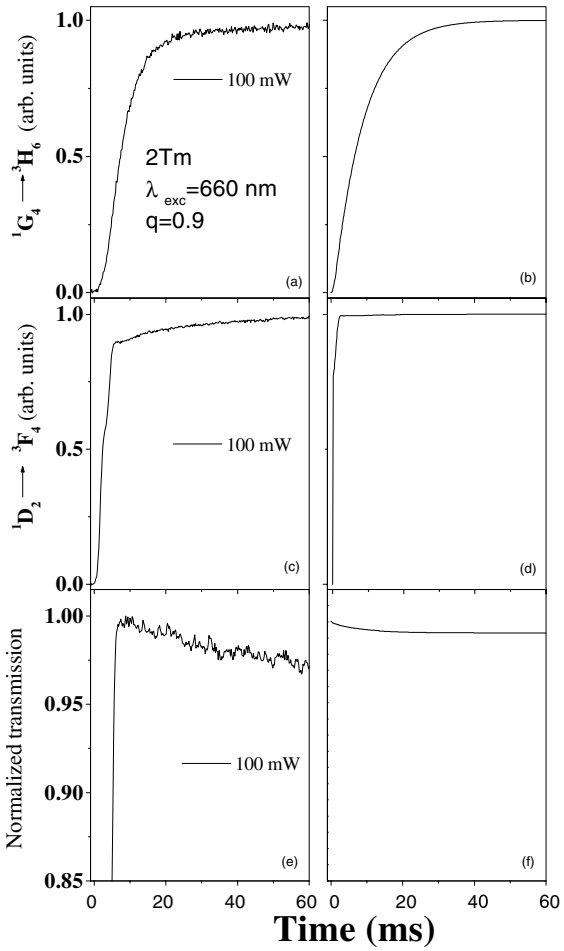

Figure 7. Experimental transient upconverted emission at 450 (*a*), 476 (*c*), and transmission (*e*), for sample 2Tm, pumped at 660 nm (100 mW). Curves (*b*), (*d*), and (*f*) correspond to the simulated results, respectively. The parameter q was changed to $q = 0.9$, while all other parameters remained fixed.

Moreover, there is no experimental dependence of the rise time of the 476 nm emission on laser power. A satisfactory fit to our experimental results is observed and the rate equations adequately describe the experimental results.

The ESA represented by R_{35} in figure 1 is also responsible for some oscillations in transient transmission previously observed by other groups [37]. This effect is predicted by our rate equations when R_{35} is comparable to or greater than R_{24} and laser powers are high enough.

Different rate equations have been reported to explain PA in Tm-doped systems [25, 33–35]. References [35] and [25] proposed four-level systems which exclude the $^1D_2$ level. According to our results, information is lost if the $^1D_2$ level is not considered, because it exhibits a very peculiar behaviour in the PA regime, as shown in figure 3. Moreover, if energy migration is not considered, PA should be more pronounced in highly doped samples, at variance with our experimental results.

5. Conclusions

PA in Tm^{3+}-doped fluoroindogallate glasses has been reported. It was shown that PL emission at 476 nm is achieved under the pumping scheme, and an increase in the rise time of the $^1G_4$ level was also demonstrated. A theoretical treatment was proposed in order to explain the experimental results. It consisted of five rate equations, which included a pumping mechanism for the $^1D_2$ level and a $^3F_4$ level lifetime dependence on the Tm concentration. The rate equation parameters W_2, S_{13}, and S_{14} were allowed to vary with the Tm concentration, while the other parameters were fixed for all samples. The experimental features of the $^1D_2$, $^1G_4$ rise curves and transient transmission as a function of Tm concentration from 1 to 7 mol% were satisfactorily predicted. It was concluded that CR mechanisms are more efficient in highly doped samples, but upconversion at 476 nm is quenched and PA disappears. We attributed this behaviour to energy migration of the $^3F_4$ metastable level, which resulted in shorter lifetimes and also shifted the threshold of PA to higher laser powers.

The results presented indicate that Tm^{3+}-doped fluoroindogallate glasses may be interesting systems if one wishes to obtain blue emission at 476 nm in the photon avalanche regime as well as at 450 nm. The optimum Tm concentration for PA in these glasses is about 2 mol%.

Acknowledgments

This work was supported by Conselho Nacional de Desenvolvimento Científico e Tecnológico (CNPq), Fundação de Amparo à Pesquisa do Estado de São Paulo (FAPESP), CAPES and FINEP.

References

[1] Macfarlane R M 1994 *J. Physique Coll.* IV **45** C42 89
[2] Herbert T, Wannemacher R, Macfarlane R M and Lenth W 1992 *Appl. Phys. Lett.* **60** 2592
[3] Chivian J S, Case W E and Eden D D 1979 *Appl. Phys. Lett.* **35** 124
[4] Koch M E, Kueny A W and Case W E 1990 *Appl. Phys. Lett.* **56** 1083
[5] Chen Y H and Auzel F 1994 *Electron. Lett.* **30** 1602
[6] Auzel F, Chen Y H and Meichenin D 1994 *J. Lumin.* **60–61** 692
[7] Scheps R 1995 *IEEE J. Quantum Electron.* **31** 309
[8] Joubert M F 1999 *Opt. Mater.* **11** 181 and references therein
[9] Joubert M F, Guy S and Jacquier B 1993 *Phys. Rev.* B **48** 10 031
[10] Reisfeld R 1977 *Lasers and Excited States of Rare Earths* (New York: Springer)
[11] Hirao K, Tamai K, Tanabe S and Soga N 1993 *J. Non-Cryst. Solids* **160** 261
[12] Guy S, Joubert M F and Jacquier B 1997 *Phys. Rev.* B **55** 8240
[13] Shu Q and Rand S C 1997 *Phys. Rev.* B **55** 8776
[14] Hehlen M P, Kuditcher A, Lenef A L, Ni H, Shu Q, Rand S C, Rai J and Rai S 2000 *Phys. Rev.* B **61** 1116
[15] de Sousa D F, Zonetti L F C, Bell M J V, Lebullenger R, Hernandes A C and Nunes L A O 1999 *J. Appl. Phys.* **85** 2502
[16] Kueny A W, Case W E and Koch M E 1989 *J. Opt. Soc. Am.* B **6** 639
[17] Shen Y and Auzel F 1994 *J. Phys. D: Appl. Phys.* **27** 1
[18] Auzel F 1980 *Radiationless Processes* ed B D Bartolo (New York: Plenum) p 250
[19] Grant W J 1971 *Phys. Rev.* B **4** 648
[20] Normand C, Pomeau Y and Velarde M G 1977 *Rev. Mod. Phys.* **49** 126
[21] Guy S, Joubert M F and Jacquier B 1997 *Phys. Rev.* B **55** 8240
[22] Holstein T, Lyo S K and Orbach R 1977 *Phys. Rev.* B **15** 4693
[23] Judd B R 1962 *Phys. Rev.* **127** 750
Ofelt G S 1988 *J. Chem. Phys.* **37** 511
[24] de Sousa D F *et al* 2002 *Phys. Rev.* B **65** at press

[25] Martin I R, Rodriguez V D, Guyot Y, Guy S, Boulon G and Joubert M F 2000 *J. Phys.: Condens. Matter* **12** 1507
[26] Kishimoto S and Hirao K 1997 *J. Non-Cryst. Solids* **213** 393
[27] Oomen E W J L 1992 *J. Lumin* **50** 317
[28] Guery C, Adam J L and Lucas J 1988 *J. Lumin* **42** 181
[29] Guy S, Joubert M F and Jacquier B 1994 *Phys. Status Solidi* b **183** K33
[30] Joubert M F, Guy S, Linares C, Jacquier B and Adam J L 1995 *J. Non-Cryst. Solids* **184** 98
[31] Brenier A, Garapon C, Madej C, Pedrini C and Boulon G 1994 *J. Lumin.* **62** 147
[32] Brenier A and Jurdyc A M 1996 *J. Lumin.* **69** 131
[33] Collings B C and Silversmith A L 1994 *J. Lumin.* **62** 271
[34] Dyson J M, Jaffe S M, Eilers H, Jones M L, Dennis W M and Yen W M 1994 *J. Lumin.* **60–61** 668
[35] Silversmith A J 1994 *J. Lumin.* **62** 271
[36] Guy S, Shepherd D P, Joubert M F and Jacquier B and Poignant H 1997 *J. Opt. Soc. Am.* B **14** 926
[37] Guy S, Bonner C L, Shepherd D P, Hanna D C, Ttropper A C and Ferrand B 1998 *IEEE J. Quantum Electron* **34** 900
[38] Tanabe S, Suzuki K, Soga N and Hanada T 1995 *J. Lumin.* **65** 247